UWB Positioning with Generalized Gaussian Mixture Filters

Philipp Müller, Henk Wymeersch, *Member, IEEE,* and Robert Piché, *Member, IEEE*

Abstract—Low-complexity Bayesian filtering for nonlinear models is challenging. Approximative methods based on Gaussian mixtures (GM) and particle filters are able to capture multimodality, but suffer from high computational demand. In this paper, we provide an in-depth analysis of a generalized GM (GGM), which allows component weights to be negative, and requires significantly fewer components than the traditional GM for ranging models. Based on simulations and tests with real data from a network of UWB nodes, we show how the algorithm's accuracy depends on the uncertainty of the measurements. For nonlinear ranging the GGM filter outperforms the extended Kalman filter (EKF) in both positioning accuracy and consistency in environments with uncertain measurements, and requires only slightly higher computational effort when the number of measurement channels is small. In networks with highly reliable measurements, the GGM filter yields similar accuracy and better consistency than the EKF.

Index Terms—Bayesian filtering, Gaussian mixture, Indoor positioning, UWB

1 Introduction

Location-aware applications are enabled by positioning techniques, and are an essential feature of many commercial, public service, and military wireless networks [1], [2]. An important requirement for many applications is that they allow positioning in real time using limited energy resources and computational effort, enabling local processing on small mobile devices.

In outdoor environments, localization and navigation techniques mainly rely on Global Navigation Satellite System (GNSS) signals. However, indoors and also under forest canopies and in certain urban settings, such as urban canyons, poor signal penetration by GNSS generally results in unavailable or unreliable location information [3]. Therefore, positioning in those environments must rely on other measurements, e.g. from an inertial measurement unit (IMU) or from radio signals such as cellular networks, Bluetooth, wireless local area networks (WLAN), or ultra-wideband (UWB). In particular, UWB has attracted a great deal of interest [1], [4], [5], [6], as the use of extremely large bandwidths enables accurate range estimates and high reliability [1].

- *P. Müller and R. Piché are with the Department of Automation Science and Engineering (ASE), Tampere University of Technology, P.O. Box 692, FI-33101 Tampere, Finland.*
  E-mail: philipp.muller, robert.piche@tut.fi
- *H. Wymeersch is with the Department of Signals and Systems, Chalmers University of Technology, S-41296 Gothenburg, Sweden.*
  E-mail: henkw@chalmers.se

Philipp Müller acknowledges the financial support of the Doctoral Programme of TUT's President, and the financial support by the Finnish Doctoral Programme in Computational Sciences (FICS) and TUT-Foundation (TTY-säätiö) for his research visit to Chalmers University of Technology, Sweden. This research was supported, in part, by the European Research Council, under Grant No. 258418 (COOPNET).

To track movements in UWB networks, Bayesian filters are commonly employed [7], [8], [9]. For linear Gaussian models, the Kalman filter is optimal [7, p. 206 ff.], while in mildly nonlinear conditions the extended Kalman filter (EKF) is a popular choice [10], [11]. In contrast to these low-complexity methods, in highly nonlinear conditions computationally demanding methods such as the particle filter are required to achieve high accuracy [12]. However, for small mobile devices the particle filter is not an attractive solution due to its computational requirements. The EKF can also be employed in highly nonlinear conditions, but suffers from a number of drawbacks. In particular, the EKF can seriously underestimate the posterior covariance in highly nonlinear situations [13]. In nonlinear situations, the likelihood function can have multiple peaks. Those peaks could be captured by approximating the likelihood as a Gaussian mixture (GM) and using a Gaussian mixture filter (GMF). To reduce the complexity of the GMF, it is important to keep the number of Gaussian components as small as possible without losing significant information. With this tradeoff in mind, a generalized version of Gaussian mixture (GGM) that relaxes the non-negativity restriction on component weights has been proposed [14]. This relaxation makes the GGM more flexible and, under certain circumstances, leads to a significant reduction in the number of Gaussian components. For localization in cellular networks, it has been found in [14] that the GGM filter (GGMF) outperforms the EKF in terms of accuracy and consistency.

In this paper, we build on the work from [14], and perform an in-depth analysis of the GGMF. We study under which circumstances the GGMF

yields satisfying position accuracy, and how its parameters affect its approximation quality for the exact likelihood function. Furthermore, we examine the GGMF's computational complexity. For evaluation purposes we performed extensive simulations and tests with real data in an UWB network. The algorithm's positioning performance and complexity are compared with those of the EKF to see how the algorithms cope with highly nonlinear measurements.

This paper is organized as follows. After the problem formulation in Section 2, the mathematical fundamentals of EKF and GGM/GGMF are presented in Section 3, and their computational complexity is analyzed. Section 4 describes how to apply GGM/GGMF for isotropic Gaussian ranging models. The results and analyses of tests with simulated and measured UWB data are presented in Section 5. Section 6 concludes the paper.

Notation : We will denote by $\mathcal{N}(\mathbf{x}; \boldsymbol{\mu}, \boldsymbol{\Sigma})$ a Gaussian density function with vector mean $\boldsymbol{\mu}$ and covariance matrix $\boldsymbol{\Sigma}$. The expectation and covariance operators are written as $\mathrm{E}(\cdot)$ and $\mathrm{V}(\cdot)$, respectively. Vectors will be denoted in bold (e.g., $\mathbf{x}$) and matrices in bold capitals (e.g., $\mathbf{X}$).

2 System model

In Sections 4 and 5 we will focus on nonlinear ranging. Therefore, we consider the discrete-time nonlinear system

$$\mathbf{x}_k = \mathbf{F}_k \mathbf{x}_{k-1} + \mathbf{w}_k, \tag{1a}$$

$$\mathbf{y}_k = \mathbf{h}_k(\mathbf{x}_k) + \mathbf{v}_k, \tag{1b}$$

where the vectors $\mathbf{x}_k \in \mathbb{R}^{n_\mathbf{x}}$ and $\mathbf{y}_k \in \mathbb{R}^{n_{\mathbf{y}_k}}$ represent the state of the system and the vector of independent range measurements at time t_k, $k \in \mathbb{N}$, respectively. Examples of range measurements include received-signal-strength-based ranging [14] and time-of-arrival-based ranging [1]. The function $\mathbf{h}_k(\mathbf{x}_k)$ returns a vector of Euclidean distances between the position contained in state $\mathbf{x}_k$ and the locations $\mathbf{x}_{\mathrm{AP}}$ of reference nodes/access points (APs).

In the following we denote the probability density functions (pdf) of the errors $\mathbf{w}_k$ and $\mathbf{v}_k$ by $p_{\mathbf{w}_k}(\cdot)$ and $p_{\mathbf{v}_k}(\cdot)$, respectively. The aim of Bayesian filtering is, at every time t_k, to determine the posterior pdf $p(\mathbf{x}_k|\mathbf{y}_{1:k})$, where $\mathbf{y}_{1:k} \triangleq [\mathbf{y}_1, \ldots, \mathbf{y}_k]$ denotes the measurement history. Assuming[1] $\mathbf{w}_k$ and $\mathbf{v}_k$ to be white, mutually independent, with covariance matrices $\mathbf{Q}_k$ and diagonal (due to assumption of independent range measurements) $\mathbf{R}_k$ respectively, and independent of the initial state $\mathbf{x}_0$, the posterior can be determined recursively according to the following relations [11]:

Prediction (prior update):

$$p(\mathbf{x}_k|\mathbf{y}_{1:k-1}) = \int p(\mathbf{x}_k|\mathbf{x}_{k-1}) p(\mathbf{x}_{k-1}|\mathbf{y}_{1:k-1}) \, \mathrm{d}\mathbf{x}_{k-1}, \tag{2}$$

where the transition pdf is given by $p(\mathbf{x}_k|\mathbf{x}_{k-1}) = p_{\mathbf{w}_k}(\mathbf{x}_k - \mathbf{F}_k \mathbf{x}_{k-1})$.

Correction (posterior update):

$$p(\mathbf{x}_k|\mathbf{y}_{1:k}) \propto p(\mathbf{y}_k|\mathbf{x}_k) p(\mathbf{x}_k|\mathbf{y}_{1:k-1}), \tag{3}$$

where the likelihood is given by

$$p(\mathbf{y}_k|\mathbf{x}_k) = \prod_{j=1}^{n_{\mathbf{y}_k}} p_{v_{k,j}}(y_{k,j} - h_{k,j}(\mathbf{x}_k)). \tag{4}$$

The initial condition for the recursion is given by the pdf of the initial state $p(\mathbf{x}_0|\mathbf{y}_{1:0}) = p(\mathbf{x}_0)$. Knowledge of the posterior distribution (3) enables us to compute a state estimate that is optimal with respect to a given criterion. For example, the minimum mean-square error (MMSE) estimate is the posterior mean of $\mathbf{x}_k$ [10], [15]. In general and in the case analyzed within this paper, the conditional pdf cannot be determined analytically. The following section presents approximative methods for computing the posterior mean.

3 EKF and (Generalized) Gaussian Mixture Filter

In this section, we briefly describe the EKF. We then discuss GMF and GGMF, and quantify the complexity of the EKF and GGMF.

3.1 Extended Kalman Filter

The EKF, which applies Kalman filtering to a local linearization of the system (1), starts from a Gaussian approximation of the posterior at time t_{k-1}, with mean $\hat{\mathbf{x}}_{k-1}$ and covariance $\mathbf{P}_{k-1}$. The prediction (2) can then be solved exactly, leading to a Gaussian with mean $\hat{\mathbf{x}}_k^-$ and covariance $\mathbf{P}_k^-$, given by

$$\hat{\mathbf{x}}_k^- = \mathbf{F}_k \hat{\mathbf{x}}_{k-1},$$

$$\mathbf{P}_k^- = \mathbf{F}_k \mathbf{P}_{k-1} \mathbf{F}_k^T + \mathbf{Q}_k.$$

The correction step is based on a linearized measurement equation, leading to a Gaussian with posterior mean $\hat{\mathbf{x}}_k$ and posterior covariance matrix $\mathbf{P}_k$, given by

$$\hat{\mathbf{x}}_k = \hat{\mathbf{x}}_k^- + \mathbf{K}_k \left(\mathbf{y}_k - \mathbf{h}_k(\hat{\mathbf{x}}_k^-) \right)$$

$$\mathbf{P}_k = \mathbf{P}_k^- - \mathbf{K}_k \mathbf{H}_k \mathbf{P}_k^-,$$

where $\mathbf{K}_k$ denotes the optimal Kalman gain

$$\mathbf{K}_k = \mathbf{P}_k^- \mathbf{H}_k \left(\mathbf{H}_k \mathbf{P}_k^- \mathbf{H}_k^T + \mathbf{R}_k \right)^{-1}$$

1. It is straightforward to modify the paper's filters to deal with less restrictive assumptions but for the sake of simplicity we stay with these standard textbook assumptions, which are sufficient for our experimental setup.

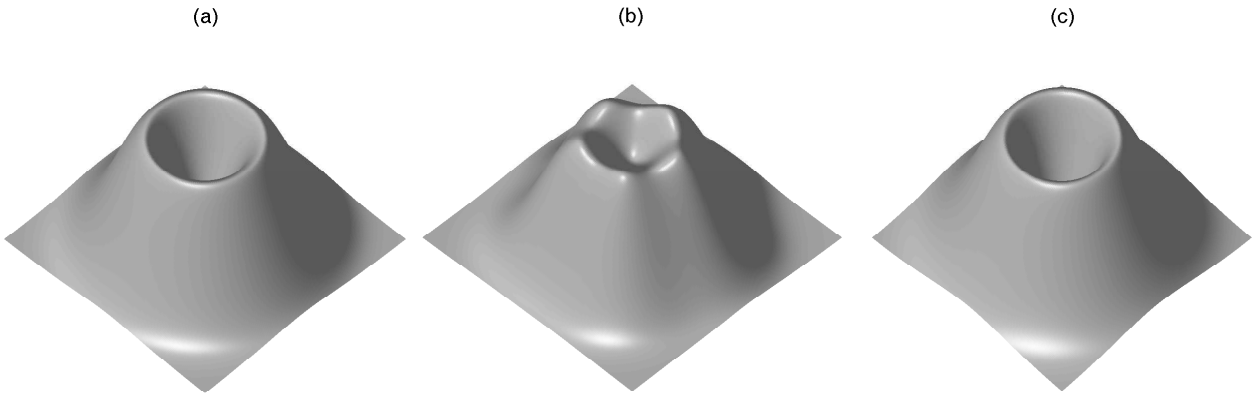

Fig. 1. Visualization of exact likelihood and approximations by GM and GGM: Subfigure (a) shows the exact normalized likelihood for a two-dimensional isotropic ranging model. The AP is in the center of the volcano-shaped likelihood and the "volcano's" brow corresponds to a circle with the range measurement as radius around the AP location. Subfigure (b) shows the approximation of the normalized likelihood by a GM with five components, and subfigure (c) shows the approximation of the normalized likelihood by a GGM with two components.

and $\mathbf{H}_k$ is obtained from the linearization of the measurement model around $\hat{\mathbf{x}}_k^-$:

$$\mathbf{H}_k = \left.\frac{\partial \mathbf{h}_k(\mathbf{x}_k)}{\partial \mathbf{x}_k}\right|_{\hat{\mathbf{x}}_k^-}.$$

It is known that in highly nonlinear situations the EKF can significantly underestimate the posterior covariance [13].

3.2 Gaussian Mixture Filter

In our context, the GMF also assumes a Gaussian state distribution at time t_{k-1}, with mean $\hat{\mathbf{x}}_{k-1}$ and covariance $\mathbf{P}_{k-1}$. Hence, the prediction step will be the same as with EKF, leading to a Gaussian distribution $\mathcal{N}(\mathbf{x}_k;\ \hat{\mathbf{x}}_k^-, \mathbf{P}_k^-)$.

The GMF then approximates the likelihood function (4) as follows: each of the $n_{\mathbf{y}_k}$ factors in (4) is approximated by a Gaussian mixture with N_j components ($j \in \{1, \ldots, n_{\mathbf{y}_k}\}$). The product of these mixtures is then a GM with $N = \prod_j N_j$ components. That GM is then multiplied with the prior, leading to a posterior with N components, with means $\boldsymbol{\mu}_i$, covariances $\boldsymbol{\Sigma}_i$, and weights $\lambda_i \in [0, 1]$. Before moving on to the next time step, this Gaussian mixture is collapsed to a single Gaussian. This can be done by moment matching, using the following formulas (derived in [14]) for the mean and covariance of the GM:

$$\mathrm{E}(\mathbf{x}) = \sum_{i=1}^{N} \lambda_i \boldsymbol{\mu}_i \triangleq \boldsymbol{\mu} \tag{5}$$

$$\mathrm{V}(\mathbf{x}) = \sum_{i=1}^{N} \lambda_i \left(\boldsymbol{\Sigma}_i + (\boldsymbol{\mu}_i - \boldsymbol{\mu})(\boldsymbol{\mu}_i - \boldsymbol{\mu})^T\right). \tag{6}$$

Clearly, the complexity of this approach is prohibitive when $n_{\mathbf{y}_k}$ or N_j are large.

Fig. 1 (b) visualizes the principle of GMs for a two-dimensional isotropic Gaussian ranging model, which will be considered in Sections 4 and 5. In order to approximate the normalized likelihood $p(y_{k,j}|\mathbf{x}_k)$ in Fig. 1 (a) we have to pick N_j peaks of the exact likelihood and use them as mean values for the GM's N_j Gaussian components. Since the exact likelihood has an infinite number of peaks (the "volcano" brow in Fig. 1 (a)) we need to find a tradeoff between approximation quality and required computational resources.

Comment: Instead of collapsing to a single Gaussian after each correction step, more complex methods can be considered. Possible methods for reduction include forgetting and merging [16], [17], [18], [19], Gaussian Mixture Reduction via Clustering (GMRC) [20], and iterative compression algorithms [21]. For a broader overview we refer the reader to [22] and references therein. However, those reduction methods generally are only suitable for Gaussian mixtures with non-negative component weights.

3.3 Generalized Gaussian Mixture Filter

The GGMF addresses the complexity issue of the GMF by approximating likelihood functions associated with ranging measurements using a normalized mixture of only two Gaussians, but allowing *negative* weights. Thus, the likelihood of ranging measurement $y_{k,j}$ is approximated as

$$\begin{aligned} p(y_{k,j}|\mathbf{x}_k) \quad &\approx \quad \mathcal{N}(\mathbf{m}_1(y_{k,j});\ \boldsymbol{\mu}_{k,j}^{(1)}, \boldsymbol{\Sigma}_{k,j}^{(1)}) \\ &\quad \cdot \left(1 - \bar{c} \cdot \mathcal{N}(\mathbf{m}_2(y_{k,j});\ \boldsymbol{\mu}_{k,j}^{(2)}, \boldsymbol{\Sigma}_{k,j}^{(2)})\right) \end{aligned} \tag{7}$$

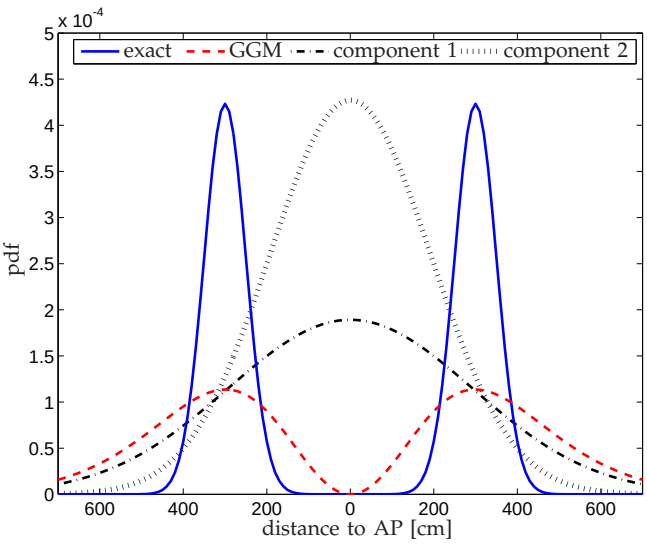

Fig. 2. Basic idea of GGM: Approximate a normalized likelihood (solid line) by a difference of two Gaussians (dashed line). Component 1 (dash-dotted line) gets positive weight, component 2 (dotted line) negative weight. The figure displays the projection of the normalized likelihood for an two-dimensional isotropic ranging model along its radial direction.

where $\bar{c} = c \cdot (2\pi)^{\frac{n_2}{2}} \sqrt{\det(\mathbf{\Sigma}_{k,j}^{(2)})}$, $c \leq 1$, and $\mathbf{m}_1(y_{k,j})$ and $\mathbf{m}_2(y_{k,j})$ are known functions of the measurements. If $\bar{c} = 0$ and $\mathbf{m}_1(y_{k,j}) = y_{k,j}$ then the conventional Kalman Filter computes the analytic solution. Using the approximate likelihood (7) yields a Gaussian mixture with possibly negative weights. However, all weights still have to sum up to one when the GM is normalized. Furthermore, parameter $\bar{c}$ ensures that such a likelihood is always nonnegative and therefore is a valid likelihood.

Fig. 1 (c) and Fig. 2 visualize the GGM's principle for an two-dimensional isotropic Gaussian ranging model. Instead of using some of the normalized likelihood's peaks (the "volcano" hilltop enclosure in Fig. 1 (c)), the GGM uses the "volcano" center, i.e. the AP location, as mean value for its two Gaussian components. More insights on how to use GGM for isotropic Gaussian ranging models will be presented in Section 4.1. The advantage of GGM compared with GM for the considered likelihood can be seen in Fig. 1. While the GGM approximation is smoother than the GM approximation and therefore resembles the likelihood more closely it requires significantly fewer components than the GM. Fig. 2 shows the projection along the radial direction of the normalized likelihood $p(y_{k,j}|\mathbf{x}_k)$ approximated by (7). Although (7) is only a rough approximation of the likelihood, it captures the location of the pdf's peaks and its general form much better than a single Gaussian (as in the EKF) or the GM (for a two-dimensional or higher-dimensional pdf) would.

TABLE 1
Complexity comparison: Number of operations from classes addition, subtraction, multiplication, division, and other (maximum, minimum, square, square root), dependent on number of measurements $n_{\mathbf{y}_k}$.

Filter	add	sub	mult	div	other
EKF	$\mathcal{O}(n_{\mathbf{y}_k}^2)$	$\mathcal{O}(n_{\mathbf{y}_k})$	$\mathcal{O}(n_{\mathbf{y}_k}^2)$	$\mathcal{O}(n_{\mathbf{y}_k})$	$\mathcal{O}(n_{\mathbf{y}_k})$
GGMF	$\mathcal{O}(2^{n_{\mathbf{y}_k}})$	$\mathcal{O}(2^{n_{\mathbf{y}_k}})$	$\mathcal{O}(2^{n_{\mathbf{y}_k}})$	$\mathcal{O}(2^{n_{\mathbf{y}_k}})$	$\mathcal{O}(2^{n_{\mathbf{y}_k}})$
EKF[a]	340	28	424	4	24
GGMF[a]	4,556	1,022	6,316	34	80

[a] for $n_{\mathbf{y}_k} = 4$ with four-dimensional $\mathbf{x}_k$

3.4 Computational complexity

It is clear that GGMF has a complexity that is exponential in the number of measurements $n_{\mathbf{y}_k}$. However, the complexity is much reduced compared to GMF for the problem considered within this paper, and still manageable for $n_{\mathbf{y}_k} < 5$, which is a reasonable value for practical scenarios (observe that in 3D, $n_{\mathbf{y}_k} = 4$ reference nodes suffice to obtain an unambiguous position estimate). A more detailed complexity comparison between GGMF and EKF is provided in Table 1 for addition, subtraction, multiplication, division, and other operations (maximum, minimum, square and square root).

4 Parameter Selection for GGMF

In this section, we describe how to select $\mathbf{m}_1(y_{k,j})$, $\mathbf{m}_2(y_{k,j})$, $\boldsymbol{\mu}_{k,j}^{(1)}$, $\boldsymbol{\mu}_{k,j}^{(2)}$, $\mathbf{\Sigma}_{k,j}^{(1)}$ and $\mathbf{\Sigma}_{k,j}^{(2)}$ in (7) for a positioning problem with Gaussian ranging errors. Then, we describe under which conditions GGM forms a good approximation.

4.1 Ranging Models

We consider isotropic Gaussian ranging models, which are frequently used in the literature (e.g. [23]), because the antennas of our UWB radios [24] used for all experiments were omnidirectional. The ranging models may be conditioned on specific propagation environments (such as line-of-sight (LOS) or non-line-of-sight (NLOS) propagation), which we will assume to be known. Moreover, we assume the mean of the ranging error is known a priori and that the ranging error variance σ^2 does not depend on the distance for ranges up to 50 meters. All these assumptions are based on experimental results with off-the-shelf UWB radios, and will be substantiated in Section 5.1. Hence, the likelihood function associated with a ranging measurement is given by

$$p(y_{k,j}|\mathbf{x}_k) \propto \exp\left(-\frac{1}{2\sigma^2}(y_{k,j} - ||\mathbf{x}_u^{(k)} - \mathbf{x}_{\mathrm{AP}}||)^2\right), \quad (8)$$

with $\mathbf{x}_u^{(k)}$ being the position vector contained in state $\mathbf{x}_k$. We will approximate this likelihood function with

a GGM centered at $\mathbf{x}_{\text{AP}}$, meaning that $\boldsymbol{\mu}_{k,j}^{(1)} = \mathbf{x}_{\text{AP}}$ and $\boldsymbol{\mu}_{k,j}^{(2)} = \mathbf{x}_{\text{AP}}$, and $\boldsymbol{\Sigma}_{k,j}^{(1)} = \sigma_{\max}^2\mathbf{I}$ and $\boldsymbol{\Sigma}_{k,j}^{(2)} = \sigma_{\min}^2\mathbf{I}$ with $\sigma_{\min} < \sigma_{\max}$. Furthermore, $\mathbf{m}_1(y_{k,j}) = \mathbf{x}_u^{(k)}$ and $\mathbf{m}_2(y_{k,j}) = \mathbf{x}_u^{(k)}$. It remains to set $\sigma_{\min}$ and $\sigma_{\max}$.

We use a modified version of the approach used in [14] and model $\sigma_{\min}$ and $\sigma_{\max}$ as

$$\sigma_{\min} = \max\{\epsilon, \alpha y_{k,j} - \sigma\}, \tag{9}$$

$$\sigma_{\max} = \alpha y_{k,j} + \sigma, \tag{10}$$

where α is a configuration parameter that enables us to improve the approximation quality of our (normalized) GGM likelihood compared with the (normalized) exact likelihood. Thus, α can now be optimized with respect to a criterion (see Section 4.2 for an example). The value of ϵ ($\epsilon > 0$) in (9) ensures that the algorithm works also in cases where $\alpha y_{k,j} - \sigma \leq 0$. For the following analyses and tests we used $\epsilon = 0.1\,\text{cm}$.

Finally, in order to ensure nonnegativity of the likelihood, we use $c = 1$. Therefore, under the Gaussian ranging error model, the only parameter remaining to be selected is the configuration parameter α.

4.2 Dependence of Approximation Quality on Ranging Variance

From Fig. 2 and the definition of the Gaussian distribution we expect that the approximation quality of a GGM depends on the standard deviation of the ranging errors. In order to quantify this dependence, we optimized α for a wide range of $\sigma \in [1, 200]\,\text{cm}$. Optimization was performed so as to minimize the Kullback-Leibler divergence (KLD) [25] between the normalized GGM likelihood and the normalized exact likelihood. Recall that the KLD between a PDF $p(\cdot)$ and a PDF $q(\cdot)$ is defined as

$$D_{\text{KL}}(p||q) = \int \ln\left(\frac{p(\mathbf{x})}{q(\mathbf{x})}\right) p(\mathbf{x})\,\mathrm{d}\mathbf{x}. \tag{11}$$

The integral (11) is evaluated numerically. Fig. 3 displays values of the KLD using α optimized by 1D line search at a range of ten meters. The results support our conjecture: as σ is increased, the KLD is reduced, meaning the GGM PDF approximates the exact PDF more accurately. For $\sigma \to 0$, the KLD blows up. Hence, for highly accurate ranging, GMM is ill-suited to approximate the exact PDF sufficiently well. In such cases it fails to model the steep probability gradients in the neighborhood of the range.

5 Simulations and Experiments

In order to get a better understanding under which circumstances the GGMF provides satisfying accuracy, we performed simulations, with models derived from experimental data, and compared the results with those of the EKF[2].

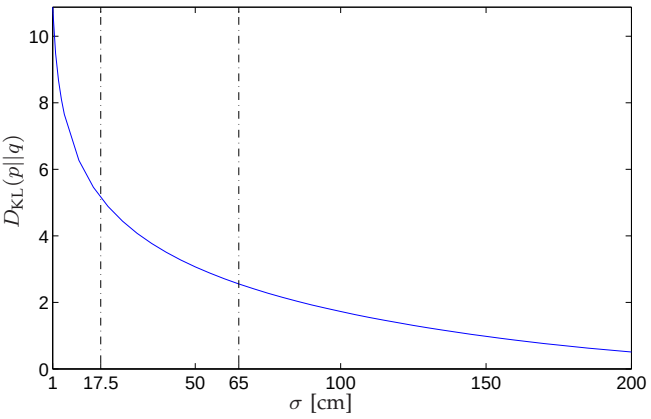

Fig. 3. Kullback-Leibler divergence (KLD) for different values of the ranging standard deviation σ using α optimized for a range of ten meters.

5.1 UWB Ranging Error Data and GGM Model

We carried out our experiments with a network of UWB radios. The radios (APs) used in our tests were Time Domain's PulsON 400 Ranging and Communications Modules (P400 RCM). They emit RF transmission from 3.1 GHz to 5.3 GHZ, with center frequency at 4.3 GHz, and provided us two-way time-of-flight (TW-TOF) ranging. Various studies have shown that in UWB networks TOA measurement noises, and thus TW-TOF measurement noises in LOS cases are usually very small [23], [26]. It has also been observed that NLOS measurements, in general, display significantly larger variances than LOS measurements [27], [28]. Therefore, we should trust LOS measurements more than NLOS measurements.

We collected $2\,225$ range measurements between ten APs placed in the known locations shown in Fig. 6, at different heights and different distances to each other. The used UWB radios have a built-in NLOS detection algorithm from which we labeled those range estimates as either LOS ($1\,745$ measurements) or NLOS (480 measurements). Note that the equipment mislabeled some measurements as LOS and mislabeled some as NLOS. From this measurement data, we determined the corresponding ranging error standard deviations, σ_{LOS} and σ_{NLOS}. Fig. 4 shows the quantile-quantile (QQ) normal

2. We also implemented a GMF and a particle filter in MATLAB. However, primarily tests showed that it would be impractical for real-time positioning on small mobile devices since the GMF requires too many components for the likelihood approximations, and the particle filter requires too many particles. For example, with just 100 particles the computation time of the particle filter was more than 60 times higher than the EKF's and approximately 8 times higher than the GGMF's computation time for the scenarios 1, 3 and 5 described in Subection 5.2

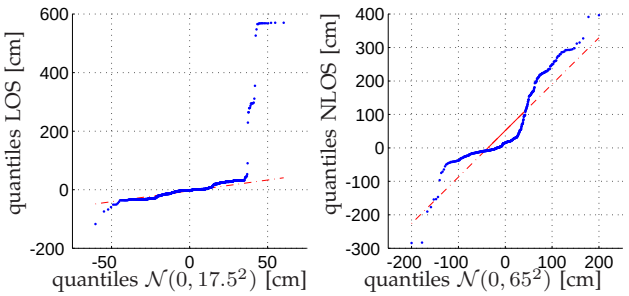

Fig. 4. QQ normal plots for errors in range estimates: The left plot shows the quantiles of ranging errors based on $1\,745$ LOS measurements versus the quantiles of a zero-mean Gaussian distribution with standard deviation $\sigma_{\text{LOS}} = 17.5\,\text{cm}$. The right plot shows the the quantiles of ranging errors based on 480 NLOS measurements versus the quantiles of a zero-mean Gaussian distribution with standard deviation $\sigma_{\text{NLOS}} = 65\,\text{cm}$.

plots that compare the quantiles of our LOS measurements (left figure) and NLOS measurements (right figure) with the quantiles of a zero-mean Gaussian distribution. Apart from a few outliers, the errors in LOS range estimates resemble such a Gaussian well. Since 68.26% of the absolute errors are smaller than $17.5\,\text{cm}$, we chose a zero-mean Gaussian distribution with standard deviation $\sigma_{\text{LOS}} = 17.5\,\text{cm}$ for modeling LOS ranging errors. In the right of the figure the QQ normal plot for the ranging errors supports the theory that NLOS measurements contain positive biases [1], and earlier findings that measurements made in NLOS conditions contain generally more outliers than measurements made in LOS condition [23]. We found that 68.44% of the absolute NLOS errors are smaller than $65\,\text{cm}$, and thus set $\sigma_{\text{NLOS}} = 65\,\text{cm}$.

Based on these values for σ_{LOS} and σ_{NLOS}, numerical minimization of the KLD at a nominal range of ten meters yielded the following optimal settings for the α parameter: $\alpha_{\text{LOS}} = 0.7374$ and $\alpha_{\text{NLOS}} = 0.7303$.

5.2 Simulation Setup

For our simulations the state

$$\mathbf{x} = \begin{bmatrix} \mathbf{x}_u \\ \mathbf{v}_u \end{bmatrix} \tag{12}$$

consisted of user position vector $\mathbf{x}_u$ and user velocity vector $\mathbf{v}_u$ in an East-North (2D) or East-North-Up (3D) coordinate system. The motion model matrix was

$$\mathbf{F}_k = \begin{bmatrix} \mathbf{I} & \Delta t\mathbf{I} \\ \mathbf{0} & \mathbf{I} \end{bmatrix}, \tag{13}$$

i.e. a constant velocity model, and the state transition noise $p_{\mathbf{w}_k} = \mathcal{N}(\mathbf{w}_k; \mathbf{0}, \mathbf{Q})$ with

$$\mathbf{Q} = 4^2 \begin{bmatrix} \frac{(\Delta t)^3}{3}\mathbf{I} & \frac{(\Delta t)^2}{2}\mathbf{I} \\ \frac{(\Delta t)^2}{2}\mathbf{I} & \Delta t\mathbf{I} \end{bmatrix}. \tag{14}$$

Within the simulations we used the time step $\Delta t = 1$ second.

In total we simulated for six different scenarios 100 tracks of 100 time steps each: scenarios 1, 3, and 5 were in 2D, where we randomly distributed four APs uniformly in a $20\,\text{m}$ by $20\,\text{m}$ square; scenarios 2, 4, and 6 were in 3D, where we distributed the four APs uniformly in a $20\,\text{m}$ by $20\,\text{m}$ by $3.5\,\text{m}$ cube. At time step $t_k = 1$ those APs had either LOS or NLOS connection to the target node on the simulated track. The range estimates were generated according to the model from Section 5.1. The LOS/NLOS condition was simulated according to a Markov jump process: at each time step, the probability of staying in a LOS condition is p_{00}, while the probability of moving from a NLOS to a LOS condition is $1 - p_{11}$. The LOS/NLOS condition of node j at time k is denoted $\beta_{k,j} \in \{\text{LOS}, \text{NLOS}\}$.

For the six different scenarios initial values for the indicator variables and transition probabilities were chosen as follows:

- Scenario 1: 2D, $\beta_{1,j} = \text{LOS}$ for $j \in \{1,2,3,4\}$, $p_{00} = p_{11} = 1$;
- Scenario 2: 3D, $\beta_{1,j} = \text{LOS}$ for $j \in \{1,2,3,4\}$, $p_{00} = p_{11} = 1$;
- Scenario 3: 2D, $\beta_{1,j} = \text{LOS}$ for $j \in \{1,2\}$ and $\beta_{1,j} = \text{NLOS}$ for $j \in \{3,4\}$, $p_{00} = p_{11} = 0.8$;
- Scenario 4: 3D, $\beta_{1,j} = \text{LOS}$ for $j \in \{1,2\}$ and $\beta_{1,j} = \text{NLOS}$ for $j \in \{3,4\}$, $p_{00} = p_{11} = 0.8$;
- Scenario 5: 2D, $\beta_{1,j} = \text{NLOS}$ for $j \in \{1,2,3,4\}$, $p_{00} = p_{11} = 1$; and
- Scenario 6: 3D, $\beta_{1,j} = \text{NLOS}$ for $j \in \{1,2,3,4\}$, $p_{00} = p_{11} = 1$.

Scenarios 1 and 2 simulate benign cases with full LOS conditions, whereas scenarios 3 and 4 simulate more realistic cases, where both LOS and NLOS measurements occur. Scenarios 5 and 6, finally, simulate harsh conditions in which we can rely only on uncertain NLOS measurements. For all tracks and all scenarios the initial position estimate for EKF and GGMF was chosen at the center of the square (2D) or cube (3D) respectively with the initial covariance matrix set to an uninformative $10^6\mathbf{I}$. Furthermore, in the GGMF the posterior GGM was approximated by one Gaussian using (5) and (6) to ensure reasonable computation time. The mean of this Gaussian was used as position estimate.

We computed in each scenario for each track and each time step the positioning error as Euclidean distance, namely

$$e_{\hat{\mathbf{x}}_u} = ||\hat{\mathbf{x}}_u - \mathbf{x}_u||_2, \tag{15}$$

where $\hat{\mathbf{x}}_u$ and $\mathbf{x}_u$ are the estimated and the true user position. For evaluation we used the following four accuracy measures:

- *Mean error:* empirical mean of all 100-by-100 two- or three-dimensional positioning errors;

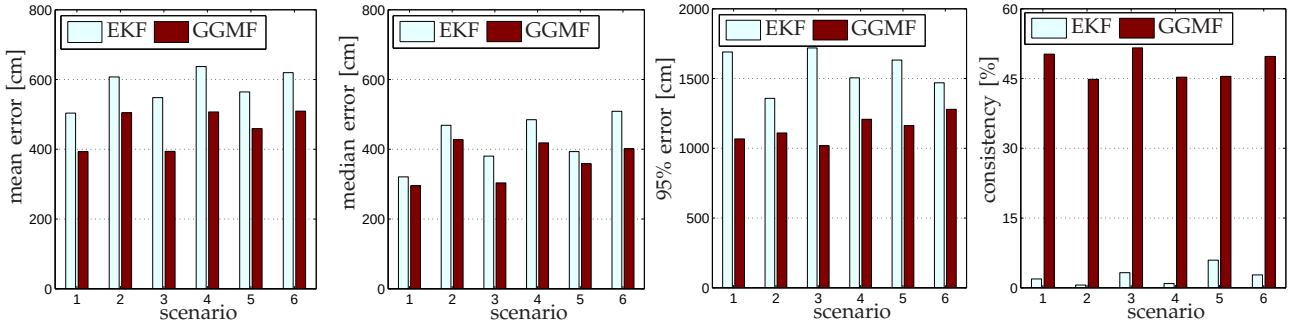

Fig. 5. Accuracy measures for simulation scenarios 1 to 6: In scenarios 1 (2D) and 2 (3D) four LOS measurements were available at every time step. In scenarios 3 (2D) and 4 (3D) at time $t_k = 1$ two LOS and two NLOS measurements were available, and their type could change at every time step according to a Markov jump process. In scenarios 5 (2D) and 6 (3D) four NLOS measurements were available at every time step.

- *Median error:* empirical median of all 100-by-100 two- or three-dimensional positioning errors;
- *95% error:* 95th percentile of all 100-by-100 two- or three-dimensional positioning errors; and
- *Consistency:* measures accuracy of the estimated position's covariance matrix; percentage of time steps for which a filter was consistent with respect to the Gaussian consistency test [10, p. 235 ff.] with risk level 5%.[3]

Comment: In our simulations neither EKF nor GGMF tested if their current position estimate was feasible (e.g., within the area in which the tracks were simulated). Using map information could significantly improve results, but is out of the scope for this paper.

5.3 Simulation Results

Fig. 5 contains the accuracy measures mean, median, 95% errors and consistency levels for all six simulation scenarios for both EKF and GGMF.

The GGMF outperforms the EKF in all six scenarios. Mean errors errors decreased 16% to 28%, median errors decreased between 8% and 21%, and 95% errors decreased 13% to 41%. Moreover, the GGMF provided significantly higher consistency levels than the EKF. However, both filters show consistency far below the desired 95%. This is expected for the EKF, since it tends to underestimate the true covariance matrix due to nonlinearities [13]. The weak consistencies for our GGMF might be a result of using the Gaussian consistency test that assumes Gaussian distributions, which does not hold in the analyzed cases. Alternatively, we could have used the general inconsistency test [13], which should report higher consistency levels for all tests with all filters.

3. In the Gaussian consistency test, for a risk level of 5%, a filter is said to be consistent at a certain time step if the estimated covariance matrix $\mathbf{P}_{k,\hat{\mathbf{x}}_u}$ of the estimated user position $\hat{\mathbf{x}}_u$ fulfills the inequality $(\hat{\mathbf{x}}_u - \mathbf{x}_u)^T \mathbf{P}_{k,\hat{\mathbf{x}}_u}^{-1} (\hat{\mathbf{x}}_u - \mathbf{x}_u) \leq \chi_2^2(0.95) = 5.9915$, where $\mathbf{x}_u$ is the true user position. In case of Gaussian posterior distribution, the closer the consistency value is to 95%, the better the covariance matrix estimation is.

We also determined the computation time of EKF and GGMF for our particular implementation. In line with our results from Section 3.4, the computation time for GGMF for all six scenarios is approximately eight times higher than for EKF.

Furthermore, we applied an unscented Kalman filter (UKF) on scenarios 1, 3 and 5 [29]. The obtained accuracy measures were very close to those of the EKF, except for better consistency (but still worse than GGMF's consistency). Furthermore, the UKF needed approximately three times more computation time than the EKF. Thus, for better readability of the figures UKF results are not shown.

5.4 Experimental Results

We now report our evaluation of EKF and GGMF with real-world data. We placed ten UWB radios as reference nodes in a gym at Chalmers University of Technology. An additional radio was carried by a person, attached to a belt at hip height, and moved along a track denoted by "ground truth", shown in Fig. 6, to collect ranging measurements. During the measurement campaign not all APs provided range estimates at each point of the track.[4] Furthermore, during our measurement campaign there were several gymnastics apparatuses in the gym, which are not marked in the map. We carried out four distinct tests:

- Test 1: two-dimensional positioning, using all reference nodes;
- Test 2: three-dimensional positioning, using all reference nodes;
- Test 3: two-dimensional positioning, using only 5 reference nodes;
- Test 4: three-dimensional positioning, using only 5 reference nodes.

For each test, we evaluated the performance in terms of our accuracy measures, shown in Table 2.

4. The UWB radios were powered by batteries, which for one radio failed to provide power for the whole test track. Since such failures can also occur in real-world applications, we decided to use this AP as long as it was functioning.

TABLE 2
Accuracy measures for tests with real data. Column *time* gives the relative computation time using a specific MATLAB implementation, scaled up in each test so that computation time for EKF is 1.

test	filter	time	mean [cm]	median [cm]	95% err. [cm]	cons.
1	EKF	1	137	87	336	4 %
1	GGMF	81	88	90	133	100 %
2	EKF	1	303	93	2 199	6 %
2	GGMF	70	99	95	160	100 %
3	EKF	1	168	75	465	10 %
3	GGMF	5	111	108	204	91 %
4	EKF	1	1 155	190	4 453	0 %
4	GGMF	5	137	135	219	88 %

In all cases, the GGMF clearly outperformed the EKF. Its consistency levels, mean and 95% errors are significantly better. However, for tests 1 to 3 the EKF yields similar or smaller median errors. Fig. 6 and 7 show how the errors and error statistics evolved for the two-dimensional positioning. Whereas the GGMF provides satisfying position estimates from the first time step on, the EKF needs several steps until it provides position estimates close to the true positions (we observed a similar behavior in our simulations). Once it yields an estimate close to the true position the EKF performs very well; even better than the GGMF. This can be explained by the fact that due to nonlinearities the EKF underestimates the true covariance matrix [13], and thus trusts its prior more than the GGMF. Furthermore, once the EKF yields a satisfying positioning estimate the approximation quality of the measurement function improves (since the linearization is performed in the prior mean), which improves the filter's positioning estimates.

Fig. 8 shows for tests 1 and 3 the square root of the trace of the posterior covariance matrices $\mathbf{P}_{k,\hat{\mathbf{x}}_u}$, which is associated to the estimated user position $\hat{\mathbf{x}}_u$. For the GGMF those values are generally above or close to the errors of the GGMF's position estimates. In tests 1 and 2 the algorithm overestimates the posterior covariance, whereas it underestimates it when using only five reference nodes. By contrast the EKF's position errors are generally significantly larger than $\|\mathbf{P}_{k,\hat{\mathbf{x}}_u}\|_2 = \sqrt{\mathrm{tr}(\mathbf{P}_{k,\hat{\mathbf{x}}_u})}$, which results in very poor consistencies for the tests and supports the earlier finding that the EKF tends to underestimate the true covariance matrix [13].

6 Conclusion

We have studied the generalized Gaussian mixture filter (GGMF), a Bayesian low-complexity localization and navigation algorithm, which can deal with significant nonlinearities. GGMF approximates the likelihood associated with range measurements in an isotropic Gaussian ranging model as a mixture of two Gaussian components, one having negative weight. For Gaussian ranging errors, we showed that the approximation quality of GGMF is improved for larger ranging error variances. Due to this, the GGMF is able to outperform the standard extended Kalman filter (EKF) in situations where large ranging errors are possible and where network geometry is poor. For scenarios with small ranging error variances the 2-component GGM captures the shape of the isotropic ranging error model only roughly, wherefore the GGMF offers only similar positioning accuracy than the EKF. Because the GGMF was originally developed for positioning using highly uncertain cellular telephone measurements, this behavior was expected. In addition, the tests showed that applying the GGMF is advantageous particularly in the starting phase of the positioning. Once a sufficiently precise position estimate is yielded, also the EKF provides satisfying position estimates, given a reasonable motion model. In all cases, the GGMF comes with an increase in computational complexity, which would allow real-time positioning on small mobile devices as long as the number of used range estimates at each time step is kept low (e.g., below 5). Our findings are corroborated with extensive simulations (based on real UWB ranging data) and experimental results.

Future work includes the extension to WLAN and Bluetooth localization, and the comparison with methods tailored to highly nonlinear conditions (e.g., fingerprinting, particle filtering). We will also

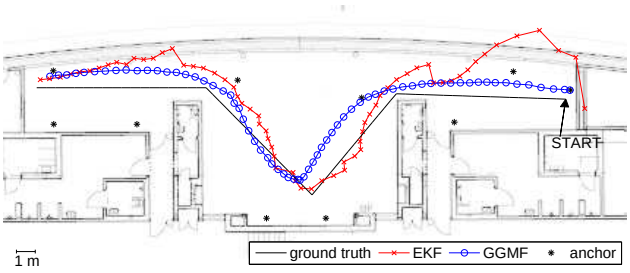

Fig. 6. Positioning in 2D using ten reference nodes (test 1).

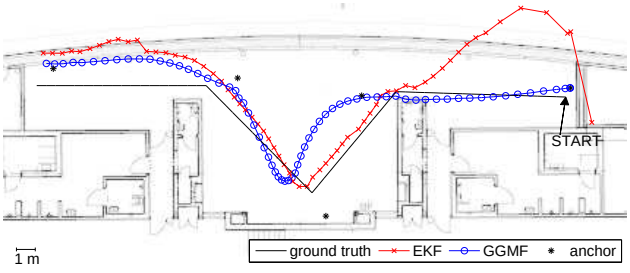

Fig. 7. Positioning in 2D using five reference nodes (test 3).

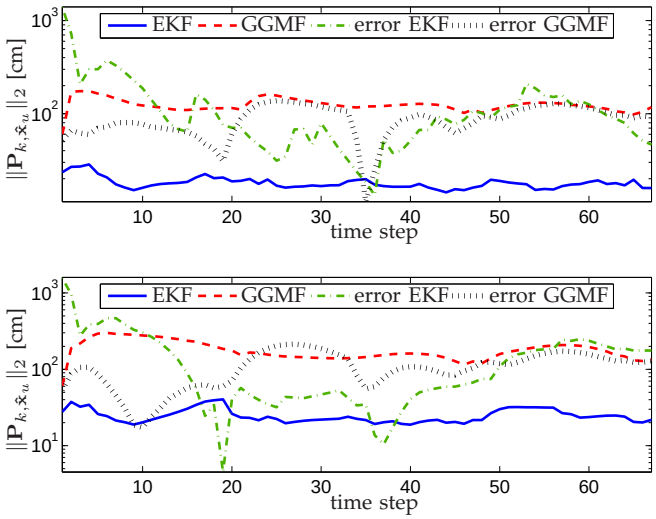

Fig. 8. $\|\mathbf{P}_{k,\hat{\mathbf{x}}_u}\|_2 = \sqrt{\text{tr}(\mathbf{P}_{k,\hat{\mathbf{x}}_u})}$ for time steps t_1 to t_{67} for test 1 (upper plot) and test 3 (lower plot) compared with positioning errors for EKF and GGMF.

investigate how GGMF can be adapted to scenarios with very small ranging error variances and other system models than the model considered within this paper, and how the complexity can be further reduced. One possible approach for handling highly reliable range measurements, which will be studied and compared with particle filters and geometric techniques in the future, is the use of other distributions, for example Student-t distributions, for the mixtures.

ACKNOWLEDGMENTS

We would like to thank Matti Raitoharju, Henri Nurminen, Simo Ali-Löytty, Juha Ala-Luhtala, and Yakup Kiliç for their careful reading of the manuscript and valuable suggestions. We are also grateful to Yakup Kiliç, Pinar Oguz Ekim, Gabriel E. Garcia, and Christopher Lindberg for their involvement in the UWB measurement campaign.

REFERENCES

[1] S. Gezici, Z. Tian, G. B. Biannakis, H. Kobayashi, A. F. Molisch, H. V. Poor, and Z. Sahinoglu, "Localization via ultra-wideband radios: a look at positioning aspects for future sensor networks," *IEEE Signal Processing Magazine*, vol. 22, no. 4, pp. 70–84, July 2005.

[2] F. Gustafsson and F. Gunnarsson, "Mobile positioning using wireless networks: possibilities and fundamental limitations based on available wireless network measurements," *IEEE Signal Processing Magazine*, vol. 22, no. 4, pp. 41–53, 2005.

[3] E. D. Kaplan, *Understanding GPS: Principles and Applications*, 2nd ed., E. D. Kaplan and C. J. Hegarty, Eds. Artech House, November 2005.

[4] D. B. Jourdan, D. Dardari, and M. Z. Win, "Position error bound for UWB localization in dense cluttered environments," *IEEE Transactions on Aerospace and Electronic Systems*, vol. 44, no. 2, pp. 613–628, April 2008.

[5] B. Alavi and K. Pahlavan, "Modeling of the TOA-based distance measurement error using UWB indoor radio measurements," *IEEE Communications Letters*, vol. 10, no. 4, pp. 275–277, April 2006.

[6] D. Dardari, A. Conti, U. Ferner, A. Giorgetti, and M. Z. Win, "Ranging with ultrawide bandwidth signals in multipath environments," *Proceedings of the IEEE*, vol. 97, no. 2, pp. 404–426, February 2009.

[7] P. S. Maybeck, *Stochastic Models, Estimation, and Control Volume 1*, ser. Mathematics in Science and Engineering. Academic Press, 1979, vol. 141.

[8] S. J. Julier and J. K. Uhlmann, "A new extension of the Kalman filter to nonlinear systems," in *Proceedings of AeroSense: the 11th international symposium on aerospace/defence sensing, simulation and controls*, 1997.

[9] L. Mihaylova, D. Angelova, S. Honary, D. Bull, C. Canagarajah, and B. Ristic, "Mobility tracking in cellular networks using particle filtering," *IEEE Transactions on Wireless Communications*, vol. 6, no. 10, pp. 3589–3599, 2007.

[10] Y. Bar-Shalom, R. X. Li, and T. Kirubarajan, *Estimation with Applications to Tracking and Navigation, Theory Algorithms and Software*. John Wiley & Sons, 2001.

[11] A. H. Jazwinski, *Stochastic Processes and Filtering Theory*, ser. Mathematics in Science and Engineering. Academic Press, 1970, vol. 64.

[12] M. S. Arulampalam, S. Maskell, N. Gordon, and T. Clapp, "A tutorial on particle filters for online nonlinear/non-Gaussian Bayesian tracking," *IEEE Transactions on Signal Processing*, vol. 50, no. 2, pp. 174–188, 2002.

[13] S. Ali-Löytty, N. Sirola, and R. Piché, "Consistency of three Kalman filter extensions in hybrid navigation," in *Proceedings of The European Navigation Conference GNSS 2005*, Munich, Germany, Jul. 2005.

[14] P. Müller, S. Ali-Löytty, M. Dashti, H. Nurminen, and R. Piché, "Gaussian mixture filter allowing negative weights and its application to positioning using signal strength measurements," in *9th Workshop on Positioning Navigation and Communication (WPNC)*, 2012, pp. 71–76.

[15] B. Ristic, S. Arulampalam, and N. Gordon, *Beyond the Kalman Filter, Particle Filters for Tracking Applications*. Boston, London: Artech House, 2004.

[16] S. Ali-Löytty and N. Sirola, "Gaussian mixture filter in hybrid navigation," in *Proceedings of The European Navigation Conference GNSS 2007*, May 2007, pp. 831–837.

[17] S. Ali-Löytty, "Gaussian mixture filters in hybrid positioning," Ph.D. dissertation, Tampere University of Technology, August 2009. [Online]. Available: http://URN.fi/URN:NBN:fi:tty-200905191055

[18] H. W. Sorenson and D. L. Alspach, "Recursive Bayesian estimation using Gaussian sums," *Automatica*, vol. 7, no. 4, pp. 465–479, July 1971.

[19] D. J. Salmond, "Mixture reduction algorithms for target tracking," *State Estimation in Aerospace and Tracking Applications, IEE Colloquium on*, pp. 7/1–7/4, 1989.

[20] D. Schieferdecker and M. F. Huber, "Gaussian mixture reduction via clustering," in *12th International Conference on Information Fusion (FUSION '09)*, 2009, pp. 1536–1543.

[21] D. F. Crouse, P. Willett, K. Pattipati, and L. Svensson, "A look at Gaussian mixture reduction algorithms," in *Proceedings of the 14th International Conference on Information Fusion (FUSION)*, 2011, pp. 1–8.

[22] M. Kristan, D. Skočaj, and A. Leonardis, "Incremental learning with Gaussian mixture models," in *Computer Vision Winter Workshop 2008, Janez Perš (ed.)*, 2008, pp. 25–32.

[23] H. Wymeersch, J. Lien, and M. Z. Win, "Cooperative localization in wireless networks," *Proceedings of the IEEE*, vol. 97, no. 2, pp. 427–450, 2009.

[24] "P400 RCM data sheet," July 2011. [Online]. Available: http://www.timedomain.com/datasheets/320-0289BP400RCMDataSheetFinal.pdf

[25] T. M. Cover and J. A. Thomas, *Elements of Information Theory*, 1st ed. New York, NY, 10158: John Wiley & Sons, 1991.

[26] Z. Low, J. Cheong, C. Law, W. Ng, and Y. Lee, "Pulse detection algorithm for line-of-sight (LOS) UWB ranging applications," *IEEE Antennas and Wireless Propagation Letters*, vol. 4, pp. 63–67, 2005.

[27] M. I. Silventoinen and T. Rantalainen, "Mobile station emergency locating in GSM," in *Proceedings of IEEE International Conference on Personal Wireless Communications*, 1996, pp. 232–238.

[28] M. P. Wylie and J. Holtzman, "The non-line of sight problem in mobile location estimation," in *Proc. 5th IEEE Int. Conf. Universal Personal Communications*, September 1996, pp. 827–831.

[29] E. Wan and R. V. der Merwe, "The unscented Kalman filter," in *Kalman filtering and neural networks*, S. Haykin, Ed. Wiley, 2001, ch. 7.

Philipp Müller received the M.Sc. degree in Mathematics in 2010 from the Chemnitz University of Technology, Germany. He is currently a Ph.D. student in the Department of Automation Science and Engineering at Tampere University of Technology, Finland. His research interests are algorithms for low-complexity localization.

Henk Wymeersch (S'99, M'05) received the Ph.D. degree in Electrical Engineering/Applied Sciences in 2005 from Ghent University, Belgium. He is currently an Associate Professor with the Department of Signals and Systems at Chalmers University of Technology, Sweden. He is also affiliated with the FORCE research center on fiber-optic communication, and is the PI of COOPNET an ERC project on cooperative networks. Prior to joining Chalmers, he was a Postdoctoral Associate with the Laboratory for Information and Decision Systems (LIDS) at the Massachusetts Institute of Technology (MIT). He is a member of the IEEE, served as Associate Editor for IEEE COMMUNICATION LETTERS (2009–2013) and the TRANSACTIONS ON EMERGING TELECOMMUNICATIONS TECHNOLOGIES (2011–present). He served as Guest Editor for EURASIP JOURNAL ON WIRELESS COMMUNICATIONS AND NETWORKING (special issue on Localization in Mobile Wireless and Sensor Networks), and for EURASIP JOURNAL ON ADVANCES IN SIGNAL PROCESSING (special Issue on Signal Processing Techniques for Anywhere, anytime positioning). He has co-authored over 100 contributions in journals and international conferences, and is the author of Iterative Receiver Design (Cambridge University Press, August 2007). His research interests include algorithm design for wireless transmission, statistical inference, and iterative processing.

Robert Piché (M'10) received the Ph.D. degree in Civil Engineering in 1986 from the University of Waterloo, Canada. He is Professor in the Department of Automation Science and Engineering at Tampere University of Technology, Finland. His scientific interests are in mathematical modelling, numerical analysis, and systems theory and in applications including positioning, finance, and solid mechanics.